Production of Electron Neutrinos at Nuclear Power Reactors and the Prospects for Neutrino Physics

B. Xin,[1,2] H.T. Wong,[2,*] C.Y. Chang,[2,3] C.P. Chen,[2] H.B. Li,[2] J. Li,[4,5] F.S. Lee,[2] S.T. Lin,[2] V. Singh,[2] F. Vannucci,[6] S.C. Wu,[2] Q. Yue,[4,5] and Z.Y. Zhou[1]

(TEXONO Collaboration)

[1] *Department of Nuclear Physics, Institute of Atomic Energy, Beijing 102413, China.*
[2] *Institute of Physics, Academia Sinica, Taipei 115, Taiwan.*
[3] *Department of Physics, University of Maryland, College Park MD 20742, U.S.A.*
[4] *Institute of High Energy Physics, Chinese Academy of Science, Beijing 100039, China.*
[5] *Department of Engineering Physics, Tsing Hua University, Beijing 100084, China.*
[6] *LPNHE, Université de Paris VII, Paris 75252, France*

(Dated: February 7, 2008)

High flux of electron neutrinos(ν_e) is produced at nuclear power reactors through the decays of nuclei activated by neutron capture. Realistic simulation studies on the neutron transport and capture at the reactor core were performed. The production of ^{51}Cr and ^{55}Fe give rise to mono-energetic ν_e's at Q-values of 753 keV and 231 keV and fluxes of 8.3×10^{-4} and 3.0×10^{-4} ν_e/fission, respectively. Using data from a germanium detector at the Kuo-Sheng Power Plant, we derived direct limits on the ν_e magnetic moment and the radiative lifetime of $\mu_\nu < 1.3\times10^{-8}$ μ_B and $\tau_\nu/m_\nu > 0.11$ s/eV at 90% confidence level (CL), respectively. Indirect bounds on τ_ν/m_ν^3 were also inferred. The ν_e-flux can be enhanced by loading selected isotopes to the reactor core, and the potential applications and achievable statistical accuracies were examined. These include accurate cross-section measurements, studies of mixing angle θ_{13} and monitoring of plutonium production.

PACS numbers: 14.60.Lm, 13.15.+g, 28.41.-i

I. INTRODUCTION

Results from recent neutrino experiments provide strong evidence for neutrino oscillations due to finite neutrino masses and mixings[1, 2]. Their physical origin and experimental consequences are not fully understood. Studies on neutrino properties and interactions can shed light on these fundamental questions and constrain theoretical models necessary for the interpretation of future precision data. It is therefore motivated to explore alternative neutrino sources and new neutrino detection channels.

The theme of this paper is to study the production of electron neutrinos(ν_e) from nuclear power reactors. Fluxes derived from the "Standard Reactor" configuration were used to obtain direct limits on the neutrino properties from data taken at the Kuo-Sheng Power Plant. The hypothetical "Loaded Reactor" scenario was also studied, where selected materials were inserted to the core to substantially enhance the ν_e-flux. The detection channels and the achievable physics potentials in ideal experiments were investigated.

II. STANDARD POWER REACTOR

A. Evaluation of Electron Neutrino Fluxes

Production of electron anti-neutrinos($\bar{\nu_e}$) due to β-decays of fission products at power reactors is a well-studied process. There are standard parametrizations for the reactor $\bar{\nu_e}$ spectra[3]. The typical fission rate at the reactor core with a thermal power of P_{th} in GW is 0.3×10^{20} P_{th} s^{-1}, while an average about 6 $\bar{\nu_e}$/fission are emitted. The modeling of the $\bar{\nu_e}$ energy spectra above 3 MeV is consistent with measurements at the <5% level[4], while the low energy portion is subjected to much bigger uncertainties[5]. In a realistically achievable setting at a location 10 m from a core with P_{th}=4.5 GW, the $\bar{\nu_e}$-flux is 6.4×10^{13} $cm^{-2}s^{-1}$.

Nuclear reactors also produce ν_e via (a) electron capture or inverse beta decay of the fission products and (b) neutron activation on the fuel rods and the construction materials at the reactor core. There were unpublished studies[6] on the reactor ν_e-fluxes from early reactor experiments, indicating that they would not contribute to the background in the measurements with $\bar{\nu_e}$. We extended these studies with realistic simulations, and focused on the potentials of using them as sources to study neutrino physics.

Primary fission daughters are predominantly neutron-rich and go through β^--decays to reach stability. Direct feeding to isotopes which decay by β^+-emissions or electron capture(EC) is extremely weak, at the $\sim10^{-8}$/fission level[7]. The leading components for the ^{235}U and ^{239}Pu fissions with relative contributions r_f, fission yields Y_f and branching ratio BR for ν_e-emissions are shown in Table Ia. The average ν_e-yield per fission Y_ν is therefore $Y_\nu = r_f \cdot Y_f \cdot BR$. In addition, stable fission products can undergo (n,γ) capture to unstable states which de-

TABLE I: The leading ν_e-yields per fission ($Y_\nu = r_f \cdot Y_f \cdot BR$) from (a) direct feeding of daughters (Z,N) and (b) neutron capture on stable isotope (Z,N-1) at equilibrium conditions.

(a)

Series	(Z,N)	$Y_f(Z,N)$	Q(MeV)	BR(%)	Y_ν
^{235}U	^{86}Rb	$1.4e^{-5}$	0.53	0.005	$4.3e^{-10}$
($r_f = 0.62$)	^{87}Sr	$<1e^{-5}$	0.2	0.3	$<1.9e^{-8}$
	^{104}Rh	$7e^{-8}$	1.15	0.45	$2.0e^{-10}$
	^{128}I	$1.2e^{-8}$	1.26	6	$4.3e^{-10}$
^{239}Pu	^{128}I	$1.7e^{-6}$	1.26	6	$2.6e^{-8}$
($r_f = 0.26$)	^{110}Ag	$1.3e^{-5}$	0.88	0.3	$1.0e^{-8}$

(b)

Series	(Z,N)	Y_f(A-1)	$\sigma_{n\gamma}$(b)	Q(MeV)	BR(%)	Y_ν
^{235}U	^{104}Rh	$3.2e^{-2}$	146	1.15	0.45	$9.0e^{-5}$
($r_f = 0.62$)	^{128}I	$1.2e^{-3}$	6.2	1.26	6	$4.3e^{-5}$
	^{122}Sb	$1.2e^{-4}$	6.2	1.62	2.2	$1.6e^{-6}$
	^{110}Ag	$3e^{-4}$	89	0.88	0.3	$5.6e^{-7}$
^{239}Pu	^{128}I	$5.2e^{-3}$	6.2	1.26	6	$8.2e^{-5}$
($r_f = 0.26$)	^{104}Rh	$6.8e^{-2}$	146	1.15	0.45	$8.0e^{-5}$
	^{110}Ag	$1.1e^{-2}$	89	0.88	0.3	$8.9e^{-6}$
	^{122}Sb	$4.3e^{-4}$	6.2	1.62	2.2	$2.6e^{-6}$

cay by ν_e-emissions. The equilibrium yield of the major components[7] are shown in Table Ib. The leading contribution is from ^{103}Rh$(n,\gamma)^{104}$Rh, where the yield summed over all four fissile isotopes is $Y_\nu = 2.1 \times 10^{-4}$ ν_e/fission. However, under realistic settings in reactor operation, the time to reach equilibrium is of the order of 10 years, such that the contribution to ν_e-emissions by this channel is also small ($Y_\nu \sim 10^{-5}$).

A complete "MCNP" neutron transport simulation[8] was performed to study the effect of neutron capture on the reactor core materials, which include the fuel elements, cooling water, control rod structures and construction materials. While the layout is generic for most nuclear power reactors, the exact dimensions and material compositions were derived from the P_{th}=2.9 GW Core#1 of the Kuo-Sheng(KS) Nuclear Power Station in Taiwan, where a neutrino laboratory[10] has been built. The reactor core materials and their mass compositions are summarized in Table IIa. A homogeneous distribution of these materials inside a stainless steel containment vessel of inner radius 225 cm, height 2750 cm, and thickness 22 cm was adopted. This approximation is commonly used and has been demonstrated to be valid in reactor design studies[9]. Standard parametrizations of the "Watt" fission neutron spectra[8, 9] were adopted as input:

$$\phi_n \propto \exp(-E/a)\,\sinh(\sqrt{bE}) \qquad (1)$$

where (a,b) depend on the fission elements. The emitted neutron spectra for the fissile isotopes are depicted in Figure 1. There are on average 2.5 neutrons generated per fission with energy distribution peaked at ∼1 MeV.

TABLE II: The compositions for (a) the construction materials inside the reactor core and of the containment vessel used in the neutron capture studies, and (b) the three isotopes responsible for ν_e-emissions.

(a)

Functions	Materials	Weight (kg)
UO_2 Fuel Elements:	Total	110000
Fission Isotopes:	^{235}U	1376
	^{238}U	98688
	^{239}Pu	431
	^{241}Pu	84
Non-Fuel Materials inside		
Containment Vessel:	Total	125000
Fuel Container	Zr-Alloy	67500
Cooling	Water	42500
Control Rod Assembly†:	B_4C	479
	Stainless Steel	14100
Containment Vessel:	Stainless Steel	910000

† at complete insertion.

(b)

Materials	Compositions (%)		
	^{50}Cr	^{54}Fe	^{58}Ni
Stainless Steel SUS304	0.95	4.2	6.3
Zr-2 alloy	0.005	0.006	0.034

The neutrons are scattered in the core and eventually absorbed by either the (n,fission) processes with the fuel elements or the (n,γ) or other interactions with the core materials.

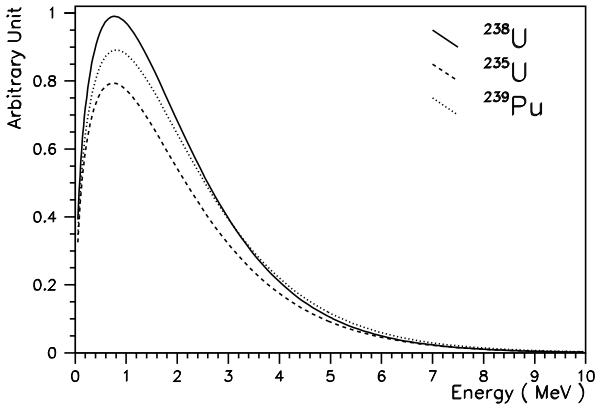

FIG. 1: The energy spectra for emitted neutrons from the fissile isotopes ^{235}U, ^{238}U and ^{239}Pu. The spectra for ^{241}Pu is approximated to be that from ^{239}Pu.

An important constraint is that an equilibrium chain reaction must be sustained to provide stable power generation. This is achieved by regulating the fraction of the control rod assembly(ξ) inserted into the fuel bundles. This constraint is parametrized by K_{eff} defined as the ratio of neutron-induced fission to starting fission rates. The variation of K_{eff} versus ξ is depicted in Figure 2.

TABLE III: The neutron capture yields Y_n of the major channels at K_{eff}=1. The average number of neutron emitted per fission is ΣY_n=2.5.

Channel	Isotope	Weight (kg)	Y_n
(n,fission) on	^{238}U	98688	0.057
fuel element	^{235}U	1376	0.62
	^{239}Pu	431	0.26
	^{241}Pu	84	0.068
		ΣY_n(fission) =	1.0
(n,γ) at	^{238}U	98688	0.59
Core Region	Water	42519	0.25
	^{10}B	5.4	0.28
	^{50}Cr	9.0	0.00067
	^{54}Fe	26.6	0.00018
	^{58}Ni	57.6	0.0010
(n,γ) at	^{50}Cr	8650	0.00016
Stainless Steel	^{54}Fe	38200	0.00012
Containment Vessel	^{58}Ni	57300	0.00026
Other capture channels:			
[mainly (n,γ) on other isotopes]			0.37
External to Containment Vessel			0.009
		ΣY_n(total) =	2.5

The equilibrium conditions require K_{eff}=1.0, and the distributions of the per-fission neutron capture yield(Y_n) are given in Table III. Only 0.35% of the neutrons escape from the containment vessel, justifying that detailed treatment exterior to the vessel is not necessary.

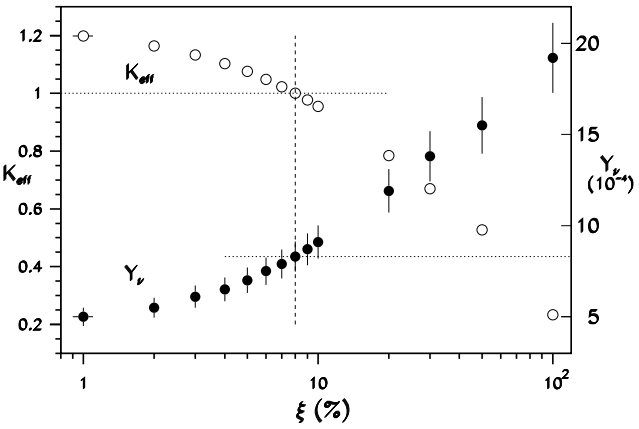

FIG. 2: The variations of the K_{eff} parameter and the neutrino yield Y_ν from ^{51}Cr, as functions of control rod fraction ξ.

Stainless steel "SUS304" and "Zr-2 alloy" are the typical construction materials at reactor cores, used in the containment vessel and control rod assembly, as well as in fuel element containers, respectively. These materials contain ^{50}Cr, ^{54}Fe and ^{58}Ni with compositions given in Table IIb. Upon activation by the (n,γ) reactions, these isotopes produce ^{51}Cr, ^{55}Fe and ^{59}Ni that will subsequently decay by EC and ν_e-emissions. Their properties (isotopic abundance IA, (n,γ) cross-sections $\sigma_{n\gamma}$, half-life $\tau_{\frac{1}{2}}$, EC Q-value and branching ratio BR) and ν_e-yield (Y_ν=Y_n·BR) are given in Table IV. The variation of Y_ν in ^{51}Cr with ξ is displayed in Figure 2. The half-life of ^{59}Ni is too long and thus not relevant for ν_e-emissions. The dominant reactor ν_e sources are therefore ^{51}Cr and ^{55}Fe, with total yields of $Y_\nu = 8.3\times10^{-4}$ and 3.0×10^{-4} ν_e/fission, implying ν_e-fluxes of 7.5×10^{16} s^{-1} and 2.7×10^{16} s^{-1}, respectively, at a 2.9 GW reactor. The total strength corresponds to a 2.7 MCi source.

TABLE IV: The ν_e sources and their yields Y_n, Y_ν(both in 10^{-4}) at the reactor core.

Isotope	IA(%)	$\sigma_{n\gamma}$(b)	$\tau_{\frac{1}{2}}$	Q(keV)	BR(%)	Y_n	Y_ν
^{103}Rh	4.6†	146	41.8 s	1145	0.45	30‡	0.14‡
^{50}Cr	4.35	15.8	27.7 d	753	100	8.3	8.3
^{54}Fe	5.85	2.3	2.73 y	231	100	3.0	3.0
^{58}Ni	68.1	4.6	7.6e^4 y	1073	100	13.0	–

† fission yield

‡ averaged over 18 months reactor period

To demonstrate the validity of the simulation procedures and results, a series of cross-checks were made. As depicted in Figure 2, the control rod fraction is ξ=8% at critical condition K_{eff}=1. The relative fission yields of the four fissile elements are given in Table III. The neutron energy spectrum averaged over the reactor core volume is depicted in Figure 3. The integrated flux is 7.6×10^{13} cm^{-2}s^{-1}, with 26%, 52% and 22% in the thermal (<1 eV), epithermal (1 eV to 1 MeV) and fast (>1 MeV) ranges, respectively. The maximal flux at the center of the reactor core is about 2.5 times the average value.

Comparisons were made between these results with industry-standard calculations and actual reactor operation data. Agreement to within 10% was achieved. In particular, the important neutron capture process ^{238}U(n,γ) leads to the accumulation of ^{239}Pu via β-decays of ^{239}U. The yield of Y_n=0.59 per fission agrees with the results from an independent study[11]. These consistency requirements posed constraints to possible systematic effects. The leading uncertainties are expected to arise from the modeling of the reactor core compositions, and were estimated to be <20%.

The process ^{238}U(n,γ) generates two $\bar{\nu}_e$'s from β-decays of ^{239}U. Adding to the 6 $\bar{\nu}_e$/fission from the fission fragments, the total $\bar{\nu}_e$-yield is therefore $Y_{\bar{\nu}}$=7.2 $\bar{\nu}_e$/fission, such that $Y_\nu/Y_{\bar{\nu}} \sim 1.6\times10^{-4}$. In particular, the ν_e-e to $\bar{\nu}_e$-e event rate ratio at the electron recoil energy range of 300 to 750 keV is $\sim 2\times10^{-4}$, too small to account for the factor of two excess over the Standard Model values in the measured $\bar{\nu}_e$-e rates recently reported by the MUNU experiment[12].

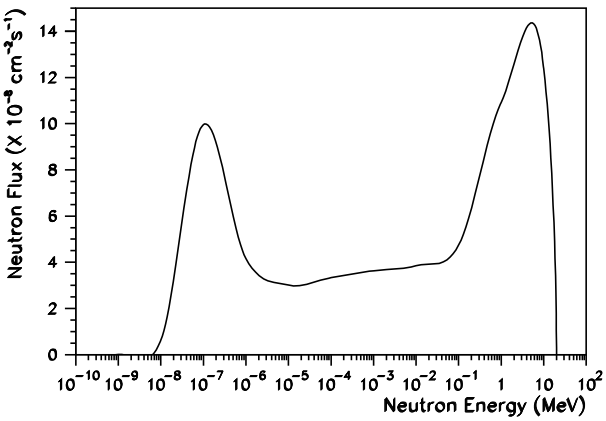

FIG. 3: Energy spectrum of neutron at the reactor core, derived from MCNP simulations.

B. Studies of Intrinsic Neutrino Properties

A high-purity germanium detector has collected data with a trigger threshold of 5 keV at a distance of 28 m from the core at KS Plant. Background at the range of 1/(kg-keV-day) was achieved[13], comparable with those from underground Dark Matter experiments. These unique low energy data provide an opportunity to study directly the possible anomalous effects from reactor $\nu_{\rm e}$. Previous reactor experiments were sensitive only to processes above the MeV range. While the sensitivities are not competitive to those from reactor $\bar{\nu_{\rm e}}$[12, 13], the studies provide direct probes on the $\nu_{\rm e}$ properties without assuming CPT invariance, and cover possible anomalous matter effects which may differentiate $\nu_{\rm e}$ from $\bar{\nu_{\rm e}}$.

The anomalous coupling of neutrinos with photons are consequences of finite neutrino masses and electromagnetic form factors[14]. The manifestations include neutrino magnetic moments (μ_ν) and radiative decays (Γ_ν). The searches of μ_ν are usually performed in neutrino-electron scattering experiments $\nu_{l_1} + {\rm e}^- \rightarrow \nu_{l_2} + {\rm e}^-$. Both diagonal and transition moments are allowed, corresponding to the cases where $l_1 = l_2$ and $l_1 \neq l_2$, respectively. The experimental observable is the kinetic energy of the recoil electrons (T). A finite neutrino magnetic moment (μ_l), usually expressed in units of the Bohr magneton

$$\mu_{\rm B} = \frac{\rm e}{2{\rm m_e}} \;\; ; \;\; {\rm e}^2 = 4\pi\alpha_{\rm em} \tag{2}$$

will contribute to a differential cross-section term given by[3]:

$$(\frac{{\rm d}\sigma}{{\rm dT}})_\mu \;=\; \frac{\pi\alpha_{\rm em}^2{\mu_l}^2}{{\rm m_e^2}}[\frac{1-{\rm T/E_\nu}}{\rm T}] \tag{3}$$

where $\alpha_{\rm em}$ is the fine-structure constant, $\rm E_\nu$ is the neutrino energy and the natural unit with $\hbar$=c=1 is adopted. The quantity μ_l is an effective parameter which can be expressed as[15]:

$$\mu_l^2 = \sum_{\rm j} \Big| \sum_{\rm k} {\rm U}_{l\rm k} \cdot \mu_{\rm jk} \Big|^2 \;, \tag{4}$$

where U is the mixing matrix and $\mu_{\rm jk}$ are the coupling constants between the mass eigenstates $\nu_{\rm j}$ and $\nu_{\rm k}$ with the photon. Experimental signatures of μ_l from reactor neutrino experiments are therefore an excess of events between reactor ON/OFF periods with an 1/T distribution.

The 18-month reactor cycle suggests that the optimal $\nu_{\rm e}$'s are from ^{51}Cr, where the half-life is $\tau_{\frac{1}{2}}$=27.7 days. The equilibrium flux at 28 m is 7.3×10^8 cm^{-2}s^{-1}. With the actual reactor OFF period denoted by t=0 to t=67 days, the background-measuring *OFF** period was taken to be from t=30 to 101 days, during which the average residual $\nu_{\rm e}$-flux was 37% of the steady-state ON-level. The ON periods included data prior to reactor OFF and starting from t=101 days. A total of 3458/1445 hours of data from the ON/*OFF** periods were used in the analysis reported in this article.

The focus in the μ_ν-search was on the T=10-100 keV range for the enhanced signal rates and robustness in the control of systematic uncertainties. The $\nu_{\rm e}$-e scattering rates due to μ_ν at the sensitivity level being explored are much larger (factor of 20 at 10 keV) than the Standard Model rates from $\bar{\nu_{\rm e}}$, such that the uncertainties in the irreducible background can be neglected[5]. Similar event selection and analysis procedures as Ref. [13] were adopted. Neutrino-induced events inside the Ge target would manifest as "lone-events" uncorrelated with the cosmic-ray veto panels and the NaI(Tl) anti-Compton scintillators. Additional pulse shape analysis further suppressed background due to electronic noise and the delayed "cascade" events. No excess of lone-events was observed in the ON$-$*OFF** residual spectrum. A limit of

$$\mu_\nu < 1.3 \times 10^{-8}\ \mu_{\rm B}$$

at 90% confidence level(CL) was derived. The residual plot and the best-fit regions are displayed in Figure 4a.

The neutrino-photon couplings probed by ν-e scatterings can also give rise to neutrino radiative decays: $\nu_{\rm j} \rightarrow \nu_{\rm k} + \gamma$ between mass eigenstates $\nu_{\rm j}$ and $\nu_{\rm k}$ with masses $\rm m_j$ and $\rm m_k$, respectively. The decay rates $\Gamma_{\rm jk}$ and half-lives $\tau_{\rm jk}$ are related to $\mu_{\rm jk}$ via[16]

$$\frac{1}{\tau_{\rm jk}} \;=\; \Gamma_{\rm jk} \;=\; \frac{\mu_{\rm jk}^2}{8\pi}\frac{({\rm m_j^2}-{\rm m_k^2})^3}{\rm m_j^3} \;. \tag{5}$$

Results from oscillation experiments[2, 17] indicate that $\nu_{\rm e}$ is predominantly a linear combination of mass eigenstates ν_1 and ν_2 with mixing angle θ_{12} given by $\sin^2\theta_{12} \sim 0.27$. The mass differences between the mass eigenstates are $\Delta{\rm m}_{12}^2 \sim 8 \times 10^{-5}$ eV^2

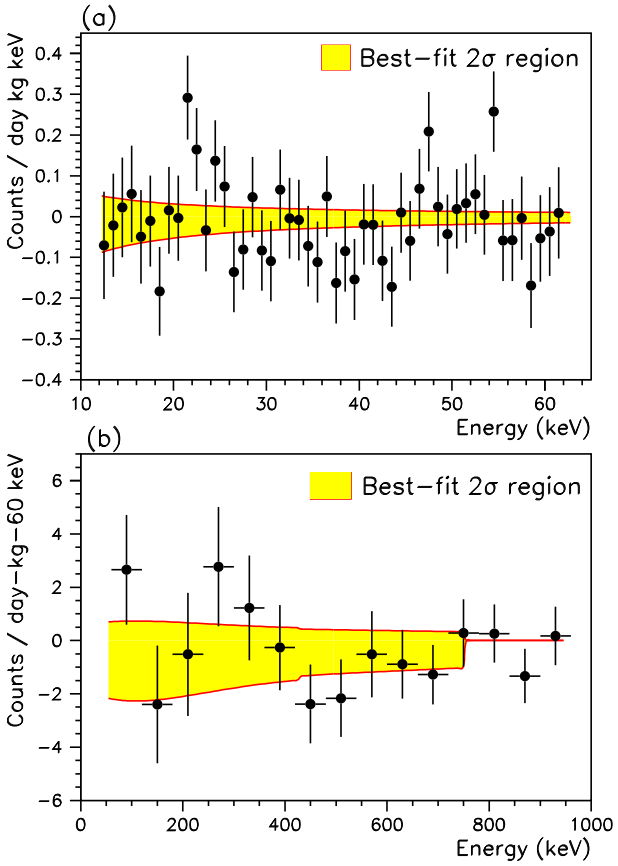

FIG. 4: Residual plots for neutrino (a) magnetic moment and (b) radiative decay searches with the reactor ^{51}Cr ν_e-source.

and $\Delta m^2_{23} \sim 2 \times 10^{-3}$ eV^2. Both "normal" (*nor.*: $m_3 \gg m_2 > m_1$) and "inverted" (*inv.*: $m_2 > m_1 \gg m_3$) mass hierarchies are allowed. The $\nu_1 \to \nu_3$ and $\nu_2 \to \nu_3$ decays are allowed only in the inverted mass hierarchy, while $\nu_2 \to \nu_1$ is possible in both hierarchies. Adopting these as input, the μ_ν limit can be translated via Eq. 5 to indirect bounds of

$$\frac{\tau_{13}}{m_1^3}(inv.: \nu_1 \to \nu_3) \;>\; 1 \times 10^{23}\ s/eV^3$$
$$\frac{\tau_{23}}{m_2^3}(inv.: \nu_2 \to \nu_3) \;>\; 4 \times 10^{22}\ s/eV^3$$
$$\frac{\tau_{21}}{m_2^3}(nor.+inv.: \nu_2 \to \nu_1) \;>\; 6 \times 10^{26}\ s/eV^3$$

at 90% CL. These limits are sensitive to the bare neutrino-photon couplings and are therefore valid for neutrino radiative decays of in vacuum.

It is also of interest to perform a direct search of $\nu_e \to \nu_X + \gamma$ the signature of which is a step-function convoluted with detector efficiencies where the end-point is at E_ν = 753 keV for ν_e's from ^{51}Cr[18]. As shown in Figure 4b, no excess of uncorrelated lone-events was observed in the residual spectrum from the ON$-OFF^*$ data. A limit of

$$\tau_\nu/m_\nu > 0.11 \text{ s/eV}$$

for ν_e at 90% CL was derived. This implies

$$\frac{\tau_1}{m_1} \;>\; 0.08\ s/eV$$
$$\frac{\tau_2}{m_2} \;>\; 0.03\ s/eV$$

in the mass eigenstate basis. These direct radiative decay limits apply to all the kinematically allowed decay channels and cover possible anomalous neutrino radiative decay mechanisms in matter, since the decay vertices are within the active detector volume. In particular, the matter-induced radiative decay rates can be enhanced by a huge factor($\sim 10^{23}$)[19] in the minimally-extended model.

Previous accelerator experiments provided the other direct "laboratory" limits on the ν_e magnetic moments and radiative decay rates: $\mu_\nu < 1.1 \times 10^{-9}\ \mu_B$[20] and $\tau_\nu/m_\nu > 6.4$ s/eV[21], both at 90% CL. The new limits from reactor ν_e are complementary to these more stringent results, since they probe parameter space with lower neutrino energy and denser target density which may favor anomalous matter effects. Astrophysical arguments[22] placed bounds which are orders of magnitude stronger[1], but there are model dependence and implicit assumptions on the neutrino properties involved[14]. Limits were also derived from solar neutrinos, through the absence of spectral distortion in the Super-Kamiokande spectra: $\mu_\nu < 1.1 \times 10^{-10}\ \mu_B$ [15, 23], and the observational limits of solar X- and γ-rays: $\tau_\nu/m_\nu > 7 \times 10^9$ s/eV [24], both at 90% CL. However, the compositions of the mass eigenstates being probed are different from those due to ν_e flavor eigenstate at the production site studied by the reactor and accelerator-based experiments, such that the interpretations of the limits are not identical.

The limits for the radiative decay lifetimes for mass eigenstates ν_1 and ν_2 from reactor and solar neutrino experiments are summarized and depicted in Figure 5, using the latest results from the neutrino experiments[2, 17] as input. The notations are defined in the figure caption. Several characteristic features can be identified. The solar neutrino experiments lead to tighter limits than those from reactor ν_e's. The indirect bounds inferred from ν_e-e scatterings are much more stringent than the direct approaches, but only apply to decays in vacuum. Among the various approaches, only the direct limit with reactor ν_e reported in this article covers decays in both vacuum and matter.

III. LOADED POWER REACTOR

A. Enhancement of Neutrino Flux

Using the simulation software discussed above, we investigated the merits of inserting selected materials to the

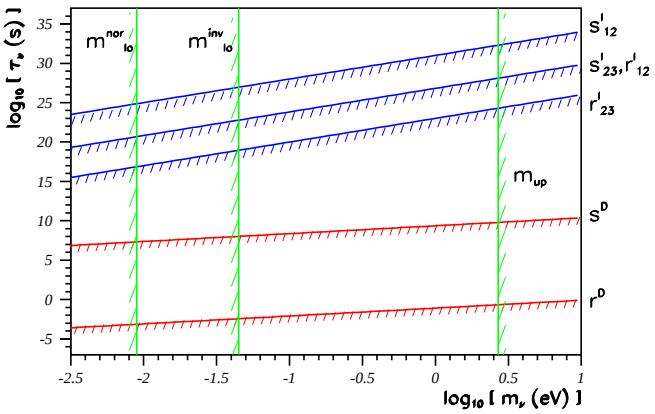

FIG. 5: Summary of the results on neutrino radiative lifetimes for ν_1 and ν_2 from reactor ν_e and solar neutrinos experiments, denoted by r and s, respectively. The superscripts (I,D) correspond to indirect bounds and direct limits, while the subscript "12" is attributed to decays driven by Δm^2_{12}, and so on. The upper bound (m_{up}) on m_ν is due to limits from direct mass measurements, while the lower bounds m^{nor}_{lo} and m^{inv}_{lo} are valid for the normal and inverted hierarchies, respectively. The indirect bounds r^I_{23} and s^I_{23} are valid for inverted hierarchy only, while r^I_{12} and s^I_{12} apply to $\nu_2 \to \nu_1$ decays in both hierarchies. All modes are valid for decays in vacuum, while r^D applies also for decays in matter. Bounds for ν_1 and ν_2 can be represented by the same bands in this scale.

reactor core to enhance the ν_e-flux. A convenient procedure is to load them to the unfilled rods or to replace part of the UO_2 fuel elements or control rod assembly during reactor outage. Though such a scenario involves difficulties with reactor operation regulations and requires further radiation safety studies, it is nevertheless technically feasible and ready − and costs much less than the various accelerator neutrino factories projects, which involve conventional neutrino beam upgrades[25], muon storage rings[26] and beta beams[27]. It is therefore of interest to explore the physics potentials and achievable sensitivities.

The candidate isotopes are those with good IA, $\sigma_{n\gamma}$ and BR as well as convenient lifetimes for the activated nuclei. In order to sustain the fission chain reactions (that is, having K_{eff}=1), the control rod fraction ξ in the core should be reduced and there is a maximum amount of the neutron-absorbing materials that can be inserted. This amount as a fraction of the fuel-element mass is denoted by Δ. Several selected materials and their maximal Δ, Y_n and Y_ν at K_{eff}=1 and ξ=0 in both natural(n) and pure(p) IA form are given in Table V. The optimal choice is ^{50}Cr(p). To illustrate how the allowed amount of control rods and source materials would relate to the reactor operation, the variations of K_{eff} and Y_ν versus Δ are plotted in Figures 6a&b, at two configurations where the control rod fractions are (a) ξ=4% and (b) ξ=0%, respectively. Criticality condition K_{eff}=1 requires a maximum load of ^{50}Cr(p) corresponding to Δ=5.4% when the control rods are completely retrieved (ξ=0%). This gives rise to a neutrino yield of Y_ν=0.31 ν_e/fission, and therefore a $Y_\nu/Y_{\bar\nu}$ ratio of 0.04. As shown in Table II, the total weight of non-fuel materials inside the containment vessel is 1.14 times that of the fuel elements. Therefore, such loading of ^{50}Cr(p) is only a small addition of materials to the reactor core. In the case of a P_{th}=4.5 GW reactor, this maximal loading implies 8900 kg of ^{50}Cr(p). A total of 4.2×10^{19} of ν_e's per second are emitted from the core, equivalent to the activity of a 1.1 GCi source. The ν_e-flux at 10 m is 3.3×10^{12} cm^{-2}s^{-1}.

TABLE V: The (n,γ) and ν_e-yields for selected materials loaded to the reactor core, at K_{eff}=1 and ξ=0%.

Isotope	IA (%)	$\sigma_{n\gamma}$ (b)	$\tau_{\frac{1}{2}}$	Q (keV)	BR (%)	Δ (%)	Y_n	Y_ν
^{50}Cr(n)	4.35	15.8	27.7 d	753	100	14.3	0.056	0.056
^{50}Cr(p)	100					5.4	0.31	0.31
^{63}Cu(n)	69.2	4.5	12.7 h	1675	61	16.3	0.20	0.12
^{63}Cu(p)	100					14.8	0.25	0.15
^{151}Eu(n)	47.8	2800	9.3 h	1920	27	0.073	0.092	0.025
^{151}Eu(p)	100					0.035	0.095	0.027

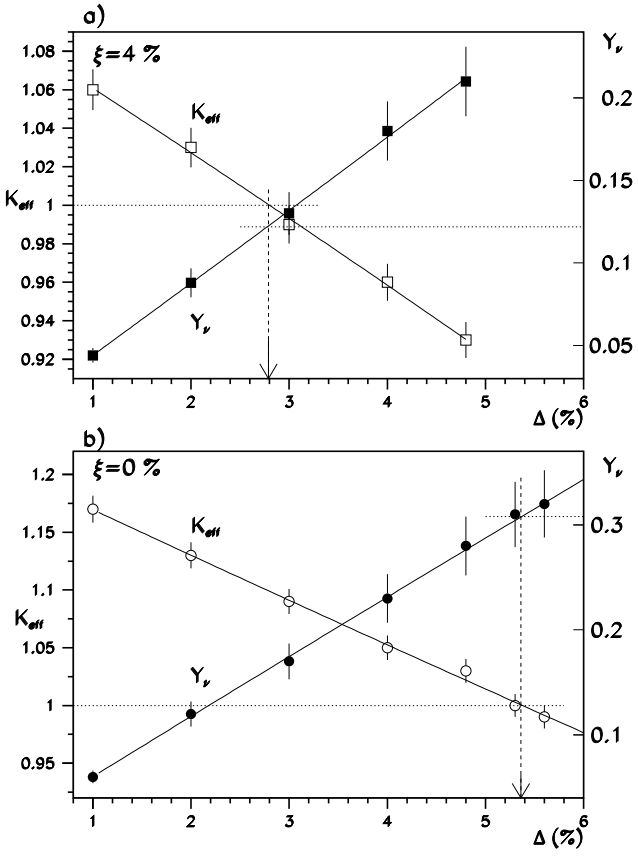

FIG. 6: The variation of the K_{eff} parameter and the neutrino yield Y_ν from ^{50}Cr(p) as a function of loading fraction Δ, at control rod fraction (a) ξ=4% and (b) ξ=0%.

TABLE VI: Expected ν_eNCC rates per ton-year at a reactor ^{51}Cr ν_e-flux of 3.3×10^{12}cm^{-2}s^{-1}(R_{core}), at the standard solar model ^{7}Be flux($R_\odot$), and due to a 1 MCi ^{51}Cr source(R_{src}).

Target	IA(%)	Threshold(keV)	R_{core}	$R_\odot$	R_{src} †
^{71}Ga	39.9	236	2100	3.8	58
^{100}Mo	9.63	168	2300	3.9	64
^{115}In	95.7	118	11000	19	300
^{176}Yb	12.7	301	3700	7.4	100

† for four half-lives of data taking.

TABLE VII: Sensitivities to θ_{13} from maximally-loaded reactor core with ^{51}Cr(p) sources for different detector options. Listed are event rates per 500-ton-year(R_{500}) for the *FAR* detector at L_0 =340 m, their achievable 1σ statistical(σ_{500}) and $\sin^2 2\theta_{13}(\delta(\sin^2 2\theta_{13}))$ accuracies.

Target	IA(%)	R_{500}	σ_{500}(%)	$\delta(\sin^2 2\theta_{13})$
^{100}Mo(n)	9.63	1900	2.3	0.027
^{100}Mo(p)	100	20000	0.71	0.0083
^{115}In(n)	95.7	9100	1.1	0.012
^{176}Yb(n)	12.7	3100	1.8	0.021
^{176}Yb(p)	100	24000	0.64	0.0075

B. Detection and Potential Applications

In order to detect such neutrinos, detection mechanisms common to both ν_e and $\bar{\nu_e}$ such as neutrino-electron scatterings are not appropriate. Instead, flavor-specific charged-current interactions (ν_eNCC) would be ideal. Solar ν_e has been observed by ν_eNCC in radiochemical experiments on ^{37}Cl and ^{71}Ga, with calibration measurements using ^{51}Cr ν_e-sources performed for ^{71}Ga[28]. Detection of the low energy solar neutrinos has been a central topic in neutrino physics. There are many detection schemes and intense research program towards counter experiments with ν_eNCC[29], using isotopes such as ^{100}Mo, ^{115}In, ^{176}Yb. The ν_eNCC rates for the various isotopes in their natural abundance at a ^{51}Cr ν_e-flux of 3.3×10^{12} cm^{-2}s^{-1} are summarized in Table VI. Also listed for comparison are the rates from the standard solar model ^{7}Be ν_e-flux and from a 1 MCi ^{51}Cr source inside a spherical detector of 1 m diameter. More than 10^4 ν_eNCC events or 1% statistical accuracy can be achieved by one ton-year of data with an indium target. Calculations of the ν_e-flux depends on the amount of loaded materials and the well-modeled reactor neutron spectra, so that a few % uncertainties should be possible. Similar accuracies can be expected on the ν_eNCC cross-section measurements. This would provide important calibration data to complement the solar neutrino program.

Such mono-energetic ν_e-sources and the detection schemes may find applications in other areas of neutrino physics. We outline two of such applications and derive their achievable statistical accuracies. Discussions on the systematic uncertainties and background of actual experiments are beyond the scope of this work, and will largely depend on the results of the ongoing research efforts to develop realistic ν_eNCC-detectors.

The first potential application is on the study of the mixing angle θ_{13}. The mono-energetic ν_e's allow simple counting experiments to be performed. The rates between *NEAR* and *FAR* detectors can be compared to look for possible deviations from $1/L^2$, L being the core-detector distance. The ν_e-flux can be accurately measured by the *NEAR* detectors, and the oscillation amplitude is precisely known at fixed Δm^2, E_ν and L. Therefore, reactor ν_e experiments are expected to have better systematic control than those with fission $\bar{\nu_e}$'s[30] where, because of the continuous energy distribution, the energy dependence in the detector response and the oscillation effects have to be taken into account. Considering both oscillation and luminosity effects, the sensitivities at a given neutrino energy E_ν depend on $[\sin^2(\frac{\Delta m^2 L}{E_\nu})]/\sqrt{L^2}$. The optimal distance for the *FAR* detector at Δm^2=0.002 eV^2 and E_ν=747 keV for the ^{51}Cr-source is therefore L_0 =340 m. Table VII shows the achievable sensitivities to $\sin^2 2\theta_{13}$ with various detector options in both natural(n) and pure(p) IA located at L_0 from a two-core power plant each with P_{th}=4.5 GW. The source strength of Y_ν=0.31 ν_e/fission for maximally-loaded ^{51}Cr in Table V is adopted. It can be seen that a ∼1% sensitivity can be statistically achieved with 5 years of data taking using a 100 ton indium target – a level comparable with those of the other reactor- and accelerator-based projects.

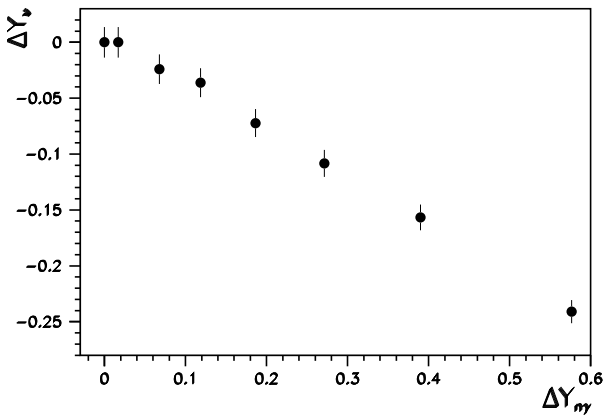

FIG. 7: Simulated correlations between the fractional changes of ν_e-yields (ΔY_ν) and those of ^{238}U(n,γ)^{239}U rates ($\Delta Y_{n\gamma}$) in the case for a ^{51}Cr source. Conditions under which the error bars are assigned are explained in the text.

Another possibility is on the monitoring of unwarranted plutonium production during reactor operation – an issue of paramount importance in the control of nuclear proliferation[31]. Plutonium is primarily produced by β-decays following ^{238}U$(n,\gamma)^{239}$U whose cross-section

is overwhelmed at high energy(>1 eV)[7]. In contrast, the (n,γ) processes in Table V which give rise to ν_e-emissions are predominantly thermal. The core neutron spectra can be modified without affecting the fission rates through optimizations of the control rod and cooling water fractions, making excessive plutonium production undetectable by monitoring the thermal power output alone. Measurements of the time-variations of the ν_eNCC event rates are effective means to probe changes in the neutron spectra, and therefore to monitor directly the ^{239}Pu accumulation rates. Illustrated in Figure 7 are the correlations between the fractional changes of the ν_e-yields (ΔY_ν) and those of the $^{238}U(n,\gamma)^{239}U$ rates ($\Delta Y_{n\gamma}$) in the case for a ^{51}Cr source having a strength of Y_ν=0.31 ν_e/fission. The uncertainties in ΔY_ν correspond to those statistically achieved with 19 days of data using a 10-ton indium detector located at 10 m from the reactor core. Such a measurement is adequate to make a 3σ detection on a 4% reduction of the ν_e-flux, which corresponds to a 10% enhancement of the ^{239}Pu production rate.

ACKNOWLEDGMENTS

The authors are grateful to Drs. Z.L. Luo and Y.Q Shi for discussions on reactor neutron simulations. This work was supported by contracts 91-2112-M-001-036 and 92-2112-M-001-057 from the National Science Council, Taiwan, and 19975050 from the National Science Foundation, China.

* Corresponding Author: htwong@phys.sinica.edu.tw

[1] See the respective sections in *Review of Particle Physics*, Phys. Lett. **B 592**, 1 (2004), for details and references.
[2] *Proc. of the XXI Int. Conf. on Neutrino Phys. & Astrophys., Paris*, eds. J. Dumarchez, T. Patzak, and F. Vannucci, Nucl. Phys. **B** (Proc. Suppl.) **143** (2005).
[3] P.Vogel and J.Engel, Phys. Rev. **D 39**, 3378 (1989).
[4] B. Achkar et al., Phys. Lett. **B 374**, 243 (1996).
[5] H.B. Li and H.T. Wong, J. Phys. **G 28**, 1453 (2002).
[6] S.M. Blankenship, Internal Report, UC Irvine, unpublished (1976); K. Schreckenbach, Internal Report, ILL Grenoble, unpublished (1984).
[7] Evaluation and Compilation of Fission Yields, T.R. England and B.F. Rider, ENDF-349, LA-UR-94-3106 (1993).
[8] A General Monte Carlo N-particle Transport Code, Version 4A, J. F. Briesmeister ed., LA-12625-M (1997).
[9] W.M. Stacey, Nuclear Reactor Physics, Wiley (2001).
[10] H.T. Wong, Mod. Phys. Lett. **A 19**, 1207 (2004).
[11] V.I. Kopeikin, L.A. Mikaelyan, and V.V. Sinev, Phys. Atomic Nuclei **60**, 172 (1997).
[12] Z. Daraktchieva et al., Phys. Lett. **B 564**, 190 (2003).
[13] H.B. Li et al., Phys. Rev. Lett. **90**, 131802 (2003).
[14] For a recent review, see: H.T. Wong, Nucl. Phys. **B** (Proc. Suppl.) **143**, 205 (2005).
[15] J.F. Beacom and P. Vogel, Phys. Rev. Lett. **83**, 5222 (1999).
[16] G.G. Raffelt, Phys. Rev. **D 39**, 2066 (1989).
[17] For a recent review, see: S. Goswami, A. Bandyopadhyay and S. Choubey, Nucl. Phys. **B** (Proc. Suppl.) **143**, 121 (2005).
[18] F. Vannucci, in *Proc. of Neutrino Telescope Workshop, 1999*, ed. M. Baldo-Ceolin, Vol. **1**, 165 (1999).
[19] C. Giunti, C.W. Kim, and W.P. Lam, Phys. Rev. **D 43**, 164 (1991).
[20] R.C. Allen et al., Phys. Rev. **D 47**, 11 (1993); L.B. Auerbach et al., Phys. Rev. **D 63**, 112001 (2001).
[21] D.A. Krakauer et al., Phys. Rev. **D 44**, R6 (1991).
[22] G.G. Raffelt, "Stars as Laboratories for Fundamental Physics", Sect. 7.5, U. Chicago Press (1996).
[23] D.W. Liu et al., Phys. Rev. Lett. **93**, 021802 (2004).
[24] G.G. Raffelt, Phys. Rev. **D 31**, 3002 (1985).
[25] For a recent review, see: T. Kobayashi, Nucl. Phys. **B** (Proc. Suppl.) **143**, 303 (2005).
[26] For a recent review, see: A. Tonazzo, Nucl. Phys. **B** (Proc. Suppl.) **143**, 297 (2005).
[27] For a recent review, see: M. Mezzettto, Nucl. Phys. **B** (Proc. Suppl.) **143**, 309 (2005).
[28] W. Hampel et al., Phys. Lett. **B 420**, 114 (1998); J.N. Abdurashitov et al., Phys. Rev. **C 59**, 2246 (1999).
[29] R.S. Raghavan, Phys. Rev. Lett. **37**, 259 (1976); R.S. Raghavan, Phys. Rev. Lett. **78**, 3618 (1997); H. Ejiri et al., Phys. Rev. Lett. **85**, 2917 (2000).
[30] K. Anderson et al., hep-ex/0402041 (2004).
[31] For a recent review, see: J. Learned, Nucl. Phys. **B** (Proc. Suppl.) **143**, 152 (2005).